

NUMERICAL AND EXPERIMENTAL COMPARISON OF PLASTIC WORK-HARDENING RULES

W. E. HAISLER

*Aerospace Engineering Department
Texas A & M University, College Station, Texas 77843, U.S.A.*

SUMMARY

The purpose of this paper is to describe recent numerical and experimental correlation studies of several plastic work-hardening rules. The mechanical sublayer model and the combined kinematic-isotropic hardening rules are examined and the numerical results for several structural geometries are compared to experimental results. Both monotonic and cyclic loads are considered.

The governing incremental plasticity relations are developed for both work-hardening models. The combined kinematic-isotropic hardening model is developed in terms of a ratio γ which controls the relative contribution of kinematic hardening (yield surface translation) and isotropic hardening (yield surface expansion). In addition to making use of a uniaxial stress-strain curve as input data, the model allows for the input of a yield surface size vs. uniaxial plastic strain curve obtained from a cyclic uniaxial reverse loading test.

The mechanical sublayer model is developed in general form and a new method for determining the sublayer parameters (stress weighting factors and yield stresses) is presented. It is demonstrated that former procedures used to obtain the sublayer parameters are inconsistent for multiaxial loading.

Numerical and experimental results are presented for a cylinder, circular plate with punch, and a steel pressure vessel. The numerical results are obtained with the computer program AGGIE I. The comparison study indicates that reasonable agreement is obtained with both hardening models; the choice depending upon whether the loading is monotonic or cyclic. For cyclic loading, if an experimental cyclic stress-strain curve is available, then the combined kinematic-isotropic hardening model may be used to obtain results which agree quite well with experiment.

1. Introduction

The adequacy of an elastic-plastic structural response prediction is governed to a large degree by the work-hardening model employed. The choice of a work-hardening model becomes particularly important for reverse and cyclic loading conditions. In an extensive numerical-experimental correlation study, Hunsaker, et.al. [1] compared the predictive capability of isotropic hardening, kinematic hardening, the mechanical sublayer model and the Mroz model and showed that the choice of a hardening rule depends on the material to be modeled, the anticipated loading path, and the structural behavior under consideration. Reference [1] contains a detailed description and comparison of the above mentioned hardening models; the present paper will consider primarily the combined kinematic-isotropic hardening model and the mechanical sublayer model. It should be remembered that the central purpose of most incremental plasticity theories is to obtain a relationship which predicts an increment of stress corresponding to an increment of strain (via an effective modulus). For brevity, the theoretical part of this paper concerns itself only with this aspect of elastic-plastic analysis. The development of the equations of motion, the solution of the incremental equations, the computational aspects, etc. are discussed in Refs. [2,3] and not included here.

2. Combined Kinematic-Isotropic Hardening

Possibly the first proposed hardening rule which incorporated both an expansion and translation of the yield surface during plastic flow is that presented by Edelman and Drucker [4]. The first investigator to combine classical kinematic hardening [5,6] and isotropic hardening [7] however was Hodge [8] in 1957, who proposed a linear combination of the two models. Berman and Hodge [9] later presented a very general theory of workhardening for piecewise linear yield surfaces which will reduce to combined kinematic-isotropic hardening. Hodge's most recent work on the piecewise linear yield surface theory is reported in Ref. [10].

Mroz [11,12] has introduced a fairly complicated combined kinematic-isotropic hardening rule known as the Mroz model. This model envisions a yield surface translating and expanding within a field of geometrically similar surfaces of constant moduli.

Krieg [13] developed a two surface plasticity theory which represents a form of combined kinematic-isotropic hardening. Besides a yield surface which is allowed to both expand and translate, this model also employs the concept of a "limit surface" which grows and moves independently of the enclosed yield surface. The appropriate hardening modulus is assumed to then be a function of the distance between these surfaces at the loading point.

It needs to be pointed out that the latter two models do not employ either of the classical forms (i.e. those of Ziegler [6] and Prager [5]) of yield surface translation. Rather, the translation of the yield surface is governed by the geometrical requirement that the yield surface not overlap the other geometrically similar surface employed by these models.

The form of combined kinematic-isotropic hardening used in this investigation is that presented by Tanaka [14] and Hunsaker [15]. The yield surface is assumed to translate in accordance with Ziegler's [6] rule. Both the hardening modulus and yield surface size at any point in the deformation history are assumed to be functions only of an equivalent uniaxial plastic strain. The hardening rule is formulated for small strains only.

Very recently, Key et.al. [16] have correctly extended combined kinematic-isotropic hardening to the case of large strains. Rather than relating the simple time derivative of stress to the strain rate, as is done in the current research, Ref. [16] employs the

kinematic-isotropic hardening rule with linear strainhardening to relate the corotational stress flux of the Cauchy stress to the stretching tensor. A second formulation is also proposed to relate the corotational stress flux of the Kirchhoff stress to the stretching tensor. The basis of these two models is the assumption that the stretching and Green-Lagrange strain rate may be decomposed into elastic and plastic parts. The resulting two constitutive models exhibit the necessary invariance at large strains and reduce to the formulation presented in Ref. [2].

2.1 Formulation

A fairly general form for an initial yield surface which is allowed to both translate and expand (or contract) is

$$F(S_{ij} - \alpha_{ij}) = k^2 (f d\epsilon_{ij}^P) \tag{1}$$

where $d\epsilon_{ij}^P$ is the increment of plastic strain, S_{ij} is the 2nd Piola-Kirchhoff stress tensor, ϵ_{ij} is the Green-Lagrange strain tensor, α_{ij} is the position of the center of the yield surface in stress space, and $k(f d\epsilon_{ij}^P)$ is taken to mean that the yield surface size k is a function of the history of plastic deformation.

The associated flow rule is then given by

$$d\epsilon_{ij}^P = \lambda \frac{\partial F}{\partial S_{ij}} \tag{2}$$

where λ is a scalar to be determined. Towards this end, the projection of the increment of stress onto the normal to the yield surface is a scalar multiple of the dot product of the plastic strain increment vector and the yield surface normal, or

$$dS_{ij} \frac{\partial F}{\partial S_{ij}} = c d\epsilon_{ij} \frac{\partial F}{\partial S_{ij}} \tag{3}$$

where c is scalar. Assuming small strains, for a linearly elastic material the stress increment is given by

$$dS_{ij} = E_{ijmn} (d\epsilon_{mn} - d\epsilon_{mn}^P), \tag{4}$$

where E_{ijmn} is the elastic constitutive tensor and $d\epsilon_{ij}$ is the increment of total strain. It should be emphasized that eq. (4) strictly limits the present analysis to small strains, the reason being that the simple time derivative of the stress tensor is not invariant at large strains. For large strains, a properly invariant stress flux must be employed [16]. Substituting eq.(2) into eqs.(3) and (4), and solving the resulting expression for λ ,

$$\lambda = \frac{\frac{\partial F}{\partial S_{ij}} E_{ijmn} d\epsilon_{mn}}{(E_{pqrs} \frac{\partial F}{\partial S_{rs}} + c \frac{\partial F}{\partial S_{pq}}) \frac{\partial F}{\partial S_{pq}}} \tag{5}$$

Using eqs. (2), (4), and (5), a resulting expression relating the stress increment to the total strain increment may be obtained.

$$dS_{ij} = \left(E_{ijmn} - \frac{E_{ijvw} \frac{\partial F}{\partial S_{vw}} \frac{\partial F}{\partial S_{tu}} E_{tumn}}{\frac{\partial F}{\partial S_{pq}} E_{pqrs} \frac{\partial F}{\partial S_{rs}} + c \frac{\partial F}{\partial S_{pq}} \frac{\partial F}{\partial S_{pq}}} \right) d\epsilon_{mn} \tag{6}$$

In considering the translation and expansion of the yield surface, for a point to remain on the yield surface during plastic flow,

$$\beta = \begin{cases} 0 & \text{if the material is elastic} \\ (3G)/(c/3G + 1)/k^2 & \text{if the material is plastic} \end{cases} \quad (17)$$

$$\bar{S}_{ij} = S'_{ij} - \alpha'_{ij} \quad (18)$$

$$[D^e] = 2G \begin{bmatrix} (1-\nu)/(1-2\nu) & & & & & \\ \nu/(1-2\nu) & (1-\nu)/(1-2\nu) & & & & \text{symmetric} \\ \nu/(1-2\nu) & & \nu/(1-2\nu) & & & (1-\nu)/(1-2\nu) \\ 0 & 0 & 0 & 0 & \frac{1}{2} & \\ 0 & 0 & 0 & 0 & 0 & \frac{1}{2} \\ 0 & 0 & 0 & 0 & 0 & 0 \end{bmatrix} \quad (19)$$

and G and ν are the elastic shear modulus and Poisson's ratio, respectively. The quantity \bar{S}_{ij} is termed the "active" stress and S'_{ij} and α'_{ij} are the deviatoric components of S_{ij} and α_{ij} , respectively.

For the variation of the yield surface size, k , with $\bar{\epsilon}^P$ required in eq. (1), one may use experimental data obtained from a uniaxial, cyclic reverse load test. A typical first cycle of such a test is shown in Fig. 1. Note that for subsequent cycles, one must record the accumulated $\bar{\epsilon}^P$, i.e., $\bar{\epsilon}^P = \int |d\epsilon_x^P|$. A typical k vs. $\bar{\epsilon}^P$ curve obtained from experimental cyclic stress-strain data is shown in a latter example problem. Alternately, if one makes use of the relation

$$dk = \gamma \frac{d\sigma_x}{d\epsilon_x^P} d\bar{\epsilon}^P \quad (20)$$

then an appropriate k vs. $\bar{\epsilon}^P$ curve can be generated (from the same uniaxial monotonic load test used to obtain the hardening modulus, c) and the general combined kinematic-isotropic hardening model can be specialized to pure kinematic hardening ($\gamma=0$), pure isotropic hardening ($\gamma=1$), or combined kinematic-isotropic hardening with a constant ratio, γ , of yield surface expansion (or contraction) to translation. In either the fully combined or constant ratio mode, this hardening rule can model the phenomena of cyclic strainhardening or cyclic strainsoftening, which is important in many applications.

3. Mechanical Sublayer Model

Duwez [17] in 1935 first proposed using an assemblage of elastic-perfectly plastic elements to model strainhardening behavior. Such an assemblage is termed a mechanical sublayer model. Subsequent work on this model occurred in the 1950's with investigations by White [18], Prager and Hodge [19], and Besseling [20].

Barr and Young [21] used the sublayer concept to formulate a plane stress material model with anisotropic strainhardening. Using strain controlled sublayers, initial material anisotropy is accounted for through a generalized Hooke's law. While the sublayer stress weighting factor or "area" is incorporated directly into the sublayer elasticity matrix, for an initially isotropic material the model reduces to that used in Refs. [1,19,22,23], a model which is shown herein to be inconsistent for all but uniaxial loading conditions.

Hunsaker et al. [1] compared the stress histories predicted by the mechanical sublayer model, the Mroz model, isotropic hardening, and Prager-Ziegler kinematic hardening with experiment for a variety of metals subjected to simple loading histories. The mechanical sub-

then eqs., (25), (22) and (21) yield

$$[D] = A_1[D_1] + A_2[D_2] + \dots + A_n[D_n] \quad (26)$$

Consider now the problem of determining the sublayer properties, A_α and σ_{y_α} . It is required that the mechanical sublayer model reproduce the input uniaxial tensile stress-strain curve (on which it is based) when subjected to the proper strain history. If the model is to be used solely for one dimensional stress histories, then the approach used in Refs. [1,19,22,23] is sufficient. In this case, for a piecewise linear stress-strain curve

$$A_\alpha = \frac{E_\alpha - E_{\alpha+1}}{E_1} ; \quad \sigma_{y_\alpha} = E_1 \epsilon_{11_\alpha} \quad (27)$$

where ϵ_{11_α} are the nodal strain values of the piecewise linear uniaxial stress-strain curve (see Fig. 2) and E_α is the tangent modulus of the α segment of this curve (E_1 is Young's modulus). The derivation of eq. (27) is straightforward and is presented in Refs. [2 and 3].

But suppose, as is usually the case, the aim is to use the mechanical sublayer model for multiaxial loading conditions. Then the approach just outlined is not valid. For multiaxial loading applications, the sublayer stress weighting factors and yield stresses must be obtained by subjecting the strain controlled model to the full three dimensional total strain history that accompanies the uniaxial stress-strain curve [3]. As an example, this new method of determining sublayer parameters will be outlined for the case of the piecewise curve of Fig. 2 (two strainhardening segments).

First consider the known three dimensional strain history that must accompany the uniaxial stress-strain curve. Since the material is assumed to be plastically incompressible, it is easily shown that for any point on the k^{th} linear segment of the piecewise linear curve,

$$\begin{aligned} dS_{11} &= E_k d\epsilon_{11} \\ d\epsilon_{22} &= d\epsilon_{33} = -\left[\frac{1}{2} + (\nu - \frac{1}{2}) \frac{E_k}{E_1}\right] d\epsilon_{11} \\ dS_{22} &= dS_{33} = 0. \end{aligned} \quad (28)$$

Eqs. (28) completely describe the material stress and strain history for the uniaxial stress loading.

For the mechanical sublayer model, the change from one tangent modulus to the next in Fig. 2 represents the transition of the appropriate sublayer from an elastic to a plastic state. Thus, the first sublayer will yield when the value of ϵ_{11} reaches ϵ_{11_1} , or when

$$\begin{aligned} \epsilon_{11} &= \epsilon_{11_1} \\ \epsilon_{22} &= \epsilon_{33} = -\nu \epsilon_{11_1} \end{aligned} \quad (29)$$

By substituting the stresses corresponding to eq. (29) into the von Mises yield condition and solving for the sublayer yield stress, it is easily shown that

$$\sigma_{y_1} = E_1 \epsilon_{11_1} \quad (30)$$

Sublayer two will yield when ϵ_{11} reaches ϵ_{11_2} , or when

$$\begin{aligned} \epsilon_{11} &= \epsilon_{11_2} \\ \epsilon_{22} = \epsilon_{33} &= -\nu \epsilon_{11_1} - \left[\frac{1}{2} + (\nu - \frac{1}{2}) \frac{E_2}{E_1} \right] (\epsilon_{11_2} - \epsilon_{11_1}) \end{aligned} \quad (31)$$

Note, however, that $\sigma_{y_2} \neq E_1 \epsilon_{11_2}$. Rather

$$\sigma_{y_2} = \left[\frac{3}{2} \{ (S'_{11_2})^2 + (S'_{22_2})^2 + (S'_{33_2})^2 \} \right]^{1/2} \quad (32)$$

where

$$\begin{aligned} S_{11_2} &= \frac{E}{(1+\nu)(1-2\nu)} [(1-\nu)\epsilon_{11} + \nu\epsilon_{22} + \nu\epsilon_{33}] \\ S_{22_2} = S_{33_2} &= \frac{E}{(1+\nu)(1-2\nu)} [(1-\nu)\epsilon_{22} + \nu\epsilon_{33} + \nu\epsilon_{11}] \neq 0 \end{aligned} \quad (33)$$

The determination of σ_{y_3} by noting that the third sublayer yields when $\epsilon_{11} = \epsilon_{11_3}$ is likewise straightforward.³

It is important at this point to realize that the dimension of the material stress state does not in general coincide with the dimension of the sublayer stress states. For instance, during the first piecewise linear segment of the uniaxial stress-strain curve, uniaxial stress exists in both the material and the sublayers. However, for any subsequent segment, the sublayers will be under a triaxial state of stress even though the material is still in a state of uniaxial stress.

The sublayer stress weighting factors (A_1, A_2, A_3) or "areas", are determined from the following set of algebraic equations:

$$\begin{aligned} A_1 + A_2 + A_3 &= 1 \\ dS_{22} = 0 &= dS_{22_1} A_1 + dS_{22_2} A_2 + dS_{22_3} A_3 \text{ for the } E_2 \text{ segment} \\ dS_{22} = 0 &= dS_{22_1} A_1 + dS_{22_2} A_2 + dS_{22_3} A_3 \text{ for the } E_3 \text{ segment} \end{aligned} \quad (34)$$

(dS_{22_α} refers to the dS_{22} stress increment component of the α sublayer). Or, in matrix notation,

$$[DTY]\{A\} = \{RHS\} \quad (35)$$

where for the general case of n sublayers (and hence $n-1$ strainhardening segments in the piecewise linear stress-strain curve)

$$\begin{aligned} \{A\}^T &= [A_1 \quad A_2 \quad A_3 \quad \dots \quad A_n] \\ \{RHS\}^T &= [1 \quad 0 \quad 0 \quad \dots \quad 0] \\ [DTY] &= \begin{bmatrix} 1 & 1 & 1 & \dots & 1 \\ dS_{22_1}^2 & dS_{22_2}^2 & dS_{22_3}^2 & \dots & dS_{22_n}^2 \\ dS_{22_1}^3 & dS_{22_2}^3 & dS_{22_3}^3 & \dots & dS_{22_n}^3 \\ \vdots & \vdots & \vdots & & \vdots \\ dS_{22_1}^n & dS_{22_2}^n & dS_{22_3}^n & & dS_{22_n}^n \end{bmatrix} \end{aligned} \quad (36)$$

and $dS_{22_\alpha}^j$ is the dS_{22} stress increment component of the α sublayer associated with the E_j segment of the piecewise linear stress-strain curve.

Hunsaker [3] obtained closed form solutions for the case of a two sublayer model. In this case,

$$\begin{aligned} \sigma_{y_1} &= \sigma_y \\ \sigma_{y_2} &= \frac{(1-2\nu)(E_2 - E_1)}{2(1+\nu)} \epsilon_{11_1} + \frac{3E_1 - (1 - 2\nu)E_2}{2(1 + \nu)} \epsilon_{11_2} \\ A_1 &= \frac{(E_2/E_1) - 1}{-1 + (1 - 2\nu)(E_2/E_1)/3} \end{aligned} \quad (37)$$

$$A_2 = 1 - A_1$$

As an example, suppose a two element model is to be used with

$$\nu = .3, E_2 = .5E_1, \epsilon_{11_1} = .001, \epsilon_{11_2} = .003, \text{ and } E_1 = 10 \times 10^6. \quad (38)$$

Then the values of the sublayers computed by the traditional method and the procedure just outlined are:

$$\begin{aligned} \left. \begin{aligned} A_1 &= .5 & A_2 &= .5 \\ \sigma_{y_1} &= 10000 & \sigma_{y_2} &= 30000 \end{aligned} \right\} \text{ from eq. (27)} \\ \left. \begin{aligned} A_1 &= .5357 & A_2 &= .4643 \\ \sigma_{y_1} &= 10000 & \sigma_{y_2} &= 31538.5 \end{aligned} \right\} \text{ from eq. (37)} \end{aligned}$$

For completeness, it should be noted that White [18] used the mechanical sublayer

model based on a piecewise linear shear stress-strain curve. Since for small strains, pure torsion results in only one non-zero shear strain, this approach is consistent for multi-axial loading and a formulation similar to eq. (27) may be used. The resulting model will still require a special computational procedure, such as the one given in Ref. [3], for the case of two dimensional plane stress elements. Because of the relative ease of performing an experimental uniaxial tensile test as opposed to a pure torsion test, and in view of the wide availability of such tensile data, most researchers will probably prefer to use the method of determining sublayer parameters from tensile data as just outlined [3].

4. Comparison Study

The nonlinear static analysis of several structures has been conducted using the finite element program AGGIE I which uses the plasticity models outlined herein. All solutions were obtained on the AMDAHL 470 V/6 digital computer located at the Texas A&M University Data Processing Center.

The first sample problem involves the large plastic deformation of a simply supported circular plate composed of high strainhardening 2024-0 aluminum. The plate under consideration is centrally loaded by a circular punch of radius .1875 in. to a maximum load of 4000 lbs. The dimensions of the plate are given in Fig. 3. The uniaxial material properties for this plate are given in Ref. [24] along with the plate test data and PLANS theoretical results. This particular plate is referred to as plate 4A250 in Ref. [24]. The material uniaxial stress-strain curve was approximated by five linear segments with nodal engineering stress, strain values as follows: 10,000 psi., .000995; 20,000 psi., .0131; 28,000 psi., .04502; 36,000 psi., .118; and 48,000 psi., .36311. As the value of Poisson's ratio was not specified in Ref. [24], a value of .325 was chosen for use in the plate analysis.

Using a 100 lb. load increment, the plate was modeled using eleven, and then twenty-two 8-node isoparametric continuum elements, with the results of both idealizations being the same indicating a converged solution. The execution times for the combined geometrically and materially nonlinear problem were 66.06 seconds and 206.83 seconds for the two idealizations. The predicted deflections of the lower surface of the plate at radii of 0.0 in. and 1.01 in. are presented in Fig. 3 along with theoretical and experimental data from Ref. [24].

The PLANS results shown in Fig. 3 were obtained by a finite element idealization of fourteen annular shell elements and using 5.5 lb. load increment. The fact that the annular elements of PLANS include bending effects but not the effects of transverse shear and normal stresses, whereas the elements of AGGIE I are pure continuum elements should account for the majority of the discrepancy between the results of the two codes.

It is noted that, while the theoretical results of both PLANS and AGGIE I were obtained using kinematic hardening, since the loading is monotonically increasing and each point in the structure will experience a near radial stress loading path, the results are the same as if either isotropic hardening or the mechanical sublayer model had been used.

The second problem involves the same simply supported circular plate of the preceding analysis, but subjected to a cyclic loading history of 1325 lb., then -773 lb., and finally 1325 lb. Since the loading is not monotonic, the predicted structural response will depend on the particular hardening rule used in the analysis. Based on the results of the previous sample problem, the plate was again modeled using eleven 8-node isoparametric elements. Since the loading was not severe enough to introduce appreciable geometric nonlinearities, the analyses were run as materially nonlinear only.

The structural response predicted by AGGIE I using kinematic hardening ($\gamma=0$) shown in Fig. 4 along with experimental data from Ref. [25]. The material constants included a Poisson's ratio of .325, Young's modulus of 10.05×10^6 psi, and a piecewise linear uniaxial stress-strain curve with the following nodal stress, strain values: 8,000 psi, .000796; 12,000 psi, .0025; 18,000 psi, .00925; and 35,000 psi, .10. It is seen that kinematic hardening provides for a very poor representation of structural response. The reason is as follows. During the initial loading, a large number of the integration points used in evaluating the tangent stiffness have accumulated sufficient equivalent uniaxial plastic strain to put them in regions of very low hardening modulus on the uniaxial stress-strain curve. When reyielding occurs during the load reversal, the effective modulus, eq. (16), with the low value of strainhardening modulus results in a very "soft" tangent stiffness. For a given applied load increment, the resulting displacement increment is then too large, as evidenced by the reverse loading behavior shown in Fig. 4. The slight strainhardening rate predicted by kinematic hardening after a reversal of loading has been shown in Ref. [1] to be contrary to observed material behavior. The execution time for this analysis was 81 seconds.

The results using AGGIE I and isotropic hardening ($\gamma=1$) are shown in Fig. 5. Using the same piecewise linear stress-strain curve as in the kinematic hardening analysis, the execution time for isotropic hardening was 71.2 seconds. As would be expected, since isotropic hardening predicts a reverse ideal Bauschinger effect [1] the structural response after the initial loading of 1325 lb. is predominantly elastic, resulting in poor agreement with the experimental data.

The results predicted by the mechanical sublayer model are shown in Fig. 6. Using a different piecewise linear approximation to the uniaxial stress-strain curve (8,000 psi., .00796; 16,250 psi, .00575; 25,000 psi, .02925; and 35,000 psi, .100), the execution time was 81.4 seconds on the AMDAHL 470/V6. Though agreement with experiment is still poor, because the mechanical sublayer model predicts an ideal Bauschinger effect with appreciable strainhardening after a reversal in loading [1] the predicted structural response is qualitatively much more accurate than that predicted by either kinematic or isotropic hardening for this high strainhardening material.

To provide data for comparison by future researchers, the results of constant ratio combined kinematic-isotropic hardening are presented in Figs. 7 and 8 for ratio values of $\gamma=.75$ and $\gamma=.5$, respectively. The same piecewise linear stress-strain curve used in the pure kinematic hardening analysis was employed and a compatible yield surface size-equivalent plastic strain curve was generated from eq. (20). The solution obtained for $\gamma=0.5$ is in good agreement with the experiment.

Finally, a general combined kinematic-isotropic hardening solution was obtained by using the experimental k vs. $\bar{\epsilon}^P$ curve shown in Fig. 9. This curve was obtained from an experimental, uniaxial cyclic reverse load test conducted by Winter [26]. The resulting load-deflection curve obtained by AGGIE I is shown in Fig. 10. It is seen that the results based on the experimental k vs. $\bar{\epsilon}^P$ data (variable ratio) are not quite as good as those based on a constant ratio $\gamma=0.5$. The reason for not getting better results with the experimental data is not known at this time. It may be partly due to the way in which the yield and reyield points were estimated from the cyclic stress-strain data. In this case, a .2% offset was used to define the yield and reyield points. A solution based on no offset

yielded poorer results and one would expect better results if a slightly larger offset were used to define yield.

5. Conclusions

Based on the sample problems presented and the results of the author's previous work [1], the following conclusions and recommendations on the use of combined kinematic-isotropic hardening and the mechanical sublayer model are presented.

1. For monotonic loading such that each point in the structure is subjected to a stress loading path that is nearly radial in deviatoric stress space, as in sample problem one, kinematic hardening, isotropic hardening, combined kinematic-isotropic hardening, and the mechanical sublayer model will all predict the same structural behavior. In these cases pure isotropic hardening is recommended since it should result in slightly lower execution times as fewer computations are involved.

2. For nonmonotonic loading that does not include a load reversal, isotropic hardening should be used since it has been shown [1] to best model material behavior under these conditions.

3. For load histories that include a reversal of loading, such as in sample problem two, the mechanical sublayer model should in most instances be used as it correctly predicts an ideal Bauschinger effect and appreciable strainhardening after reversed loading. If experimental data is available indicating that combined kinematic-isotropic hardening will best model the behavior of a particular material or if one is trying to model cyclic strainhardening or strainsoftening, then combined kinematic-isotropic hardening may be used.

4. In using the mechanical sublayer model for multiaxial stress loading, if the sublayer parameters are based on a uniaxial tensile stress-strain curve the procedure outlined in this paper for determining the parameters should be used.

6. Acknowledgements

This work was sponsored by George C. Marshall Spaceflight Center, NASA under Contract NAS8-31332 and by the Office of Naval Research under Contract N00014-76-C-0150

References

- [1] HUNSAKER, B., VAUGHAN, D.K., STRICKLIN, J.A., and HAISLER, W.E., "A Comparison of Current Work-Hardening Models Used in the Analysis of Plastic Deformations," Texas A&M University, Department of Aerospace Engineering, TEES-RPT-2926-73-3, Oct. 1973.
- [2] HUNSAKER, B., HAISLER, W.E., and STRICKLIN, J.A., "On the Use of Two Hardening Rules of Plasticity in Incremental and PseudoForce Analysis," in Constitutive Equations in Viscoplasticity: Computational and Engineering Aspects, AMD-Vol. 20, pp. 139-170, Winter Annual Meeting of ASME, 1976.
- [3] HUNSAKER, B., Jr., "The Application of Combined Kinematic-Isotropic Hardening and the Mechanical Sublayer Model to Small Strain Inelastic Structural Analysis by the Finite Element Method," Ph.D. Dissertation, Texas A&M University, Aug. 1976.
- [4] EDELMAN, F., and DRUCKER, D.C., "Some Extensions of Elementary Plasticity Theory," Journal of the Franklin Institute, Vol. 250, 1951, p. 581.
- [5] PRAGER, W., "The Theory of Plasticity: A Survey of Recent Achievements," Proceedings of the Institution of Mechanical Engineers, London, Vol. 169, No. 21, 1955, pp. 41-57.
- [6] ZIEGLER, H., "A Modification of Prager's Workhardening Rule," Zeitschrift fuer Angewandte Mathematik und Physik, Basel, Vol. 9a, Sept. 1958 pp. 260-276.
- [7] HILL, R., The Mathematical Theory of Plasticity, Oxford University Press, New York, 1967

- [8] HODGE, P.G., Jr., discussion of "A New Method of Analyzing Stresses and Strains in Work-Hardening Plastic Solids," W. Prager (Journal of Applied Mechanics, Vol. 23, Dec. 1956, pp. 493-496), Journal of Applied Mechanics, Vol. 24, Sept. 1957, pp. 482-483.
- [9] BERMAN, I., and HODGE, P.G., Jr., "A General Theory of Piecewise Linear Plasticity for Initially Anisotropic Materials," Nadbithka Z. Archiwum Mechaniki Stosowanej, Vol. 11, 1959, pp. 514-540.
- [10] HODGE, P.G., Jr., "Piecewise Linear Strainhardening Plasticity," in Constitutive Equations in Viscoplasticity: Computational and Engineering Aspects, AMD-Vol. 20, pp. 57-77, Winter Annual Meeting of ASME, 1976.
- [11] MROZ, Z., "On the Description of Anisotropic Workhardening," Journal of the Mechanics Physics of Solids, Vol. 15, 1967, pp. 163-175.
- [12] MROZ, Z., "An Attempt to Describe the Behavior of Metals Under Cyclic Loads Using a More General Workhardening Model," Acta Mechanica, Vol. 7, No. 2-3, 1969, pp. 199-212.
- [13] KRIEG, R.D., "A Practical Two Surface Plasticity Theory," presented at the Winter Annual Meeting of the ASME, Paper No. 75-WA/APM-12, 1975.
- [14] TANAKA, M., "Large Deflection Analysis of Elastic-Plastic Circular Plates with Combined Isotropis and Kinematic Hardening," Ingenieur-Archiv, Vol. 41, 1972, pp. 342-356.
- [15] HUNSAKER, B., Jr., "An Evaluation of Four Hardening Rules of the Incremental Theory of Plasticity," M.S. Thesis, Texas A&M University, Dec. 1973.
- [16] KEY, S.W., BIFFLE, J.H., and KRIEG, R.D., "A Study of the Computational and Theoretical Differences of Two Finite Strain Elastic-Plastic Constitutive Models," to be presented at the U.S. Germany Symposium on Finite Element.
- [17] DUWEZ, P., "On the Plasticity of Crystals," Physical Review, Vol. 47, March 1935, pp. 494-501.
- [18] WHITE, G.N., Jr., "Application of the Theory of Perfectly Plastic Solids to Stress Analysis of Strain Hardening Solids," Graduate Division of Applied Mathematics, Brown University, Tech. RPT. 5., 1950.
- [19] PRAGER, W., and HODGE, P.G., Jr., Theory of Perfectly Plastic Solids, John Wiley and Sons, Inc., New York, 1951.
- [20] BESSELING, J.F., "A Theory of Plastic Flow for Anisotropic Hardening in Plastic Deformation of an Initially Isotropic Material," National Aeronautical Research Institute, Amsterdam, Report S.4.0, 1953.
- [21] BARR, G.W., and Young, E.G., "MAT2D: A Plane Stress Material Model for an Elastic-Plastic Anisotropic Strain-Hardening Material," SC-CR-69-656, Sandia Laboratories, Albuquerque, N.M., Jan. 1970.
- [22] WU, R.W.H., and WITMER, E.A., "Finite Element Analysis of Large Elastic-Plastic Transient Deformations of Simple Structures," AIAA Journal, Vol. 9, No. 9, Sept. 1971, pp. 1719-1724.
- [23] HAISLER, W.E., STRICKLIN, J.A., and VON RIESEMANN, W.A., "DYNAPLAS - A Finite Element Program for the Dynamic Large Deflection, Elastic-Plastic Analysis of Stiffened Shells of Revolution," SLA-73-0127, Sandia Laboratories, Albuquerque, N.M. (also RPT 72-27, Aerospace Engineering Department, Texas A&M University), Dec. 1972.
- [24] WINTER, R., and LEVINE, H.S., "Experiments on Large Plastic Deformations of Circular Plates with Work Hardening," Grumman Research Department, Report RE-502, July 1975, Grumman Aerospace Corporation, Bethpage, N.Y.
- [25] LEVINE, H.S., and SVALBONAS, V., "Inelastic Nonlinear Analysis of Stiffened Shells of Revolution by Numerical Integration," Journal of Pressure Vessel Technology, May 1974, pp. 121-130.
- [26] WINTER, R., Private Communication, January 1977.

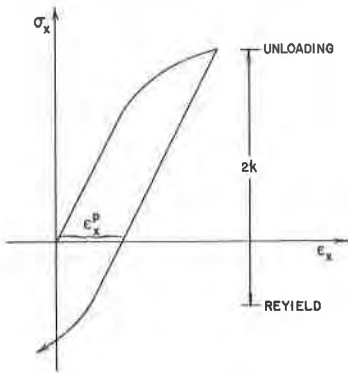


Fig. 1 The First Cycle of A Uniaxial Cyclic Loading Test

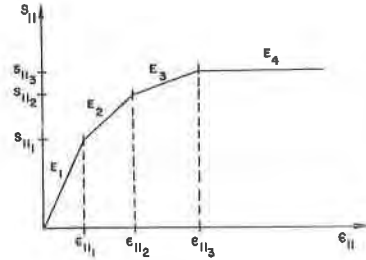


Fig. 2 A Typical Piecewise Linear Uniaxial Stress-Strain Curve

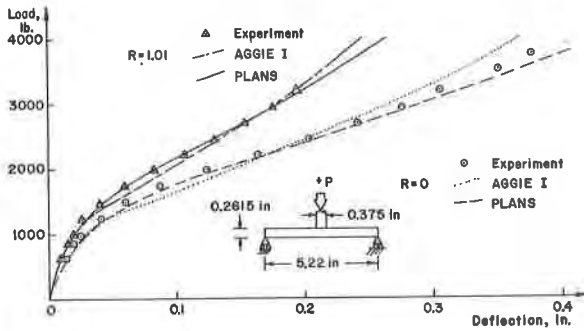


Fig. 3 Deflection History, Circular Plate with Punch

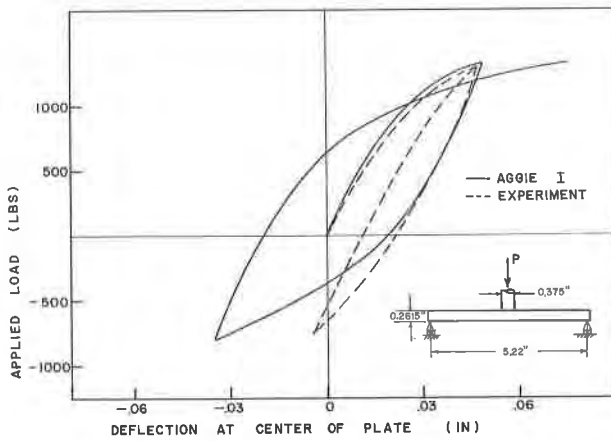


Fig. 4 Cyclic Load-Deflection Curve at Center of Circular Plate, Kinematic Hardening ($\gamma=0$)

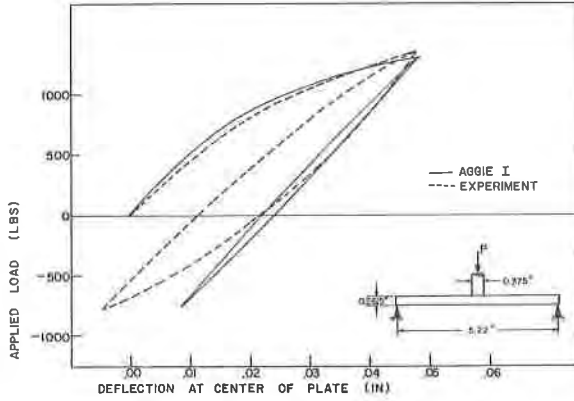


Fig. 5 Cyclic Load-Deflection Curve at Center of Circular Plate, Isotropic Hardening ($\gamma=1$)

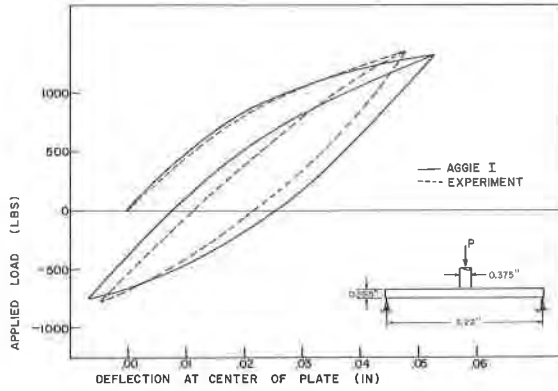


Fig. 6 Cyclic Load-Deflection Curve at Center of Circular Plate, Mechanical Sublayer Model

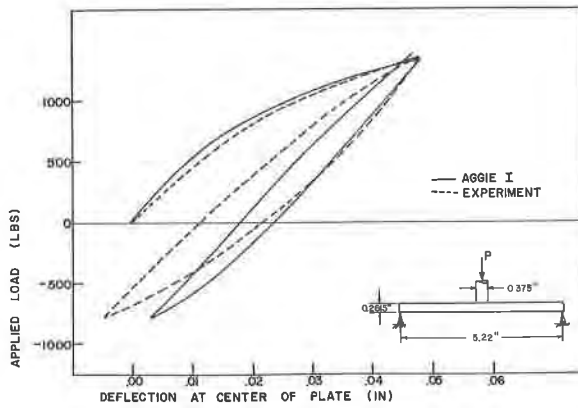


Fig. 7 Cyclic Load-Deflection Curve at Center of Circular Plate, Combined Kinematic-Isotropic Hardening, $\gamma=0.75$

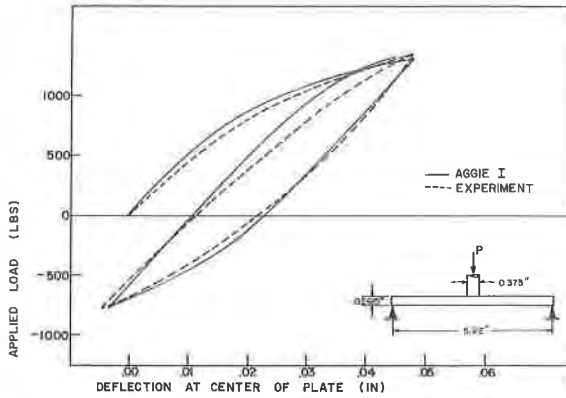


Fig. 8 Cyclic Load-Deflection Curve at Center of Circular Plate, Combined Kinematic-Isotropic Hardening, $\gamma=0.5$

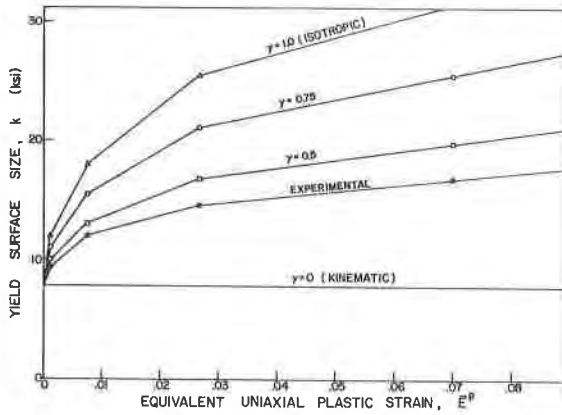


Fig. 9 Yield Surface Size vs. Equivalent Uniaxial Plastic Strain

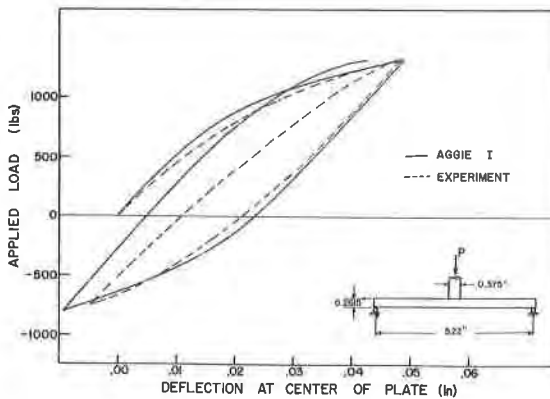


Fig. 10 Cyclic Load-Deflection Curve at Center of Circular Plate, Combined Kinematic-Isotropic Hardening, Experimental k vs. ϵ^p